

Supporting Information

Highly Efficient Molecular Nickel Catalysts for Electrochemical Hydrogen Production from Neutral Water

Peili Zhang,^a Mei Wang,^{*a} Yong Yang,^a Dehua Zheng,^a Kai Han^a and Licheng Sun^{a,b}

^a State Key Laboratory of Fine Chemicals, DUT-KTH Joint Education and Research Center on Molecular Devices, Dalian University of Technology (DUT), Dalian 116024, China. E-mail: symbueno@dlut.edu.cn; Fax: +86 411 84986245; Tel.: +86 411 84986246

^b Department of Chemistry, KTH Royal Institute of Technology, Stockholm 10044, Sweden

Materials and instruments

Materials. All manipulations for preparation and handling of organometallic complexes were carried out under pure N₂ or using high-vacuum Schlenk techniques. Diethyl ether and tetrahydrofuran were predried over activated 4 Å molecular sieves for 1 day and then distilled over sodium under N₂. Acetonitrile was distilled over CaH₂ and stored under N₂. Water was deionized with the Millipore Milli-Q UF Plus system. Electronic grad Hg (99.999%) was purchased from Aladdin. Glass carbon rods and platinum gauze were purchased from BASi for electrochemical studies. Other commercially available chemicals such as Ni(BF₄)₂·6H₂O, Co(BF₄)₂·6H₂O, Fe(BF₄)₂·6H₂O, benzaldehyde, benzyl chloride, 1,2-ethanediamine, 2,2'-diaminodiethylamine, and 2-(chloromethyl)pyridine hydrochloride were purchased from local suppliers and used as received. Complexes [(Am₂Py₃)Fe(NCCH₃)](BF₄)₂ (**4**) and [(Am₂Py₃)Co(H₂O)](BF₄)₂ (**5**) were prepared according to the previously reported protocol.^{S1,S2}

Instruments. NMR Spectra were collected with a varian INOVA 400 NMR spectrometer. Mass spectra were recorded with HP 1100 HPL/ESI-DAD-MS and Waters/Micromass LC/Q-TOF-MS instruments. Raman spectra were recorded with a DXRTM Raman Microscope

excited with a 532 nm light source. Elemental analyses were performed with a Thermoquest-Flash EA 1112 elemental analyzer.

Synthesis

Synthesis of ligands Am1Py4, Am2Py3, and Am3Py2. Ligands 1,1-di(pyridin-2-yl)-*N,N*-bis(pyridin-2-ylmethyl)methanamine (Am1Py4), *N*-benzyl-*N,N',N'*-tris(2-pyridylmethyl)ethylenediamine (Am2Py3), and *N1,N2*-dibenzyl-*N1*-(2-(benzyl(pyridin-2-ylmethyl)amino)ethyl)-*N2*-(pyridin-2-ylmethyl)ethane-1,2-diamine (Am3Py2) were prepared according to the literature procedures.^{S3,S4}

Am1Py4: ¹H NMR (CDCl₃, 400 MHz): δ 8.56 (d, *J* = 4 Hz, 2H), 8.50 (d, *J* = 4.4 Hz, 2H), 7.65 (m, 8H), 7.11 (m, 4H), 5.35 (s, 1H), 3.97 (s, 4H). ¹³C NMR (CDCl₃, 400 MHz): δ 159.87, 159.68, 149.24, 148.93, 136.45, 136.35, 123.97, 122.94, 122.14, 121.86, 71.98, and 57.20. ESI-MS: Calcd for [M+H]⁺: *m/z* 368.19; found: 368.27

Am2Py3: ¹H NMR (CDCl₃, 400 MHz): δ 8.48 (m, 3H), 7.58 (t, 3H), 7.47 (t, 3H), 7.18–7.30 (m, 5H), 7.12 (m, 3H), 3.77 (s, 4H), 3.72 (s, 2H), 3.59 (s, 2H) and 2.73 (m, 4H). ¹³C NMR (CDCl₃, 400 MHz): δ 160.16, 159.73, 148.94, 148.79, 139.18, 136.30, 128.71, 128.17, 126.88, 122.71, 122.65, 121.84, 121.78, 60.78, 60.59, 58.91, 52.20, and 51.89. ESI-MS: Calcd for [M+H]⁺: *m/z* 424.2423; found: 424.2104. Anal. Calcd for C₂₇H₂₉N₅ (%): C, 76.56; H, 6.90; N, 16.53; found: C, 76.70; H, 6.84; N 16.62.

Am3Py2: ¹H NMR (CDCl₃, 400 MHz): δ 8.48 (m, 2H), 7.58 (m, 2H), 7.44 (d, *J* = 8, 2H), 7.29–7.08 (m, 17H), 3.68 (s, 4H), 3.54 (s, 4H), 2.57 (s, 8H). ¹³C NMR (CDCl₃, 400 MHz): δ 160.23, 148.79, 139.30, 136.41, 128.85, 128.80, 128.24, 128.14, 126.95, 126.85, 122.78, 121.86, 60.56, 59.12, 59.05, 52.12, and 51.57. ESI-MS: Calcd for [M+H]⁺: *m/z* 556.3362; found: 556.3454.

Syntheses of [(Am1Py4)Ni(NCCH₃)](BF₄)₂ (1a). Complexes 1–3 were prepared with

referring to the literature procedures.^{S5,S6} Compound Ni(BF₄)₂·6H₂O (0.34 g, 1.0 mmol) was added to an acetonitrile solution (40 mL) of **Am1Py4** (0.37 g, 1.0 mmol). The mixture was stirred under nitrogen atmosphere at room temperature for 6 h. The amaranthine solution was then concentrated to ~10 mL under decreased pressure and kept under N₂ at room temperature for 2 days. Rod-shaped amaranthine crystals were obtained in a yield of 81% (0.45 g). ¹H NMR (400 MHz, CD₃COCD₃): δ 2.97, 14.31, 15.87, 38.19, 46.52, 51.67, and 53.81. TOF-MS: Calcd for [M–BF₄–NCCH₃]⁺ (C₂₃H₂₁N₅BF₄Ni): *m/z* 512.1180; found: 512.1176. Anal. Calcd for C₂₅H₂₄N₆B₂F₈Ni (%): C, 48.81; H, 3.94; N 10.95; found: C, 48.78; H, 4.01; N 11.01.

Syntheses of [(Am1Py4)Ni(H₂O)](BF₄)₂ (1b**).** The preparation of **1b** was made with an essentially identical protocol as that adopted for the preparation of **1a** but using water as solvent. The product was obtained as amaranthine crystalline solid in a yield of 70% (0.43 g). ¹H NMR (400 MHz, CD₃COCD₃): δ 3.01, 14.06, 15.69, 39.08, 46.13, and 52.07. TOF-MS: Calcd for [M–BF₄–NCCH₃]⁺ (C₂₃H₂₁N₅BF₄Ni): *m/z* 512.1180; found: 512.1171. Anal. Calcd for C₂₃H₂₃N₅OB₂F₈Ni (%): C, 46.74; H, 3.92; N, 9.08; found: C, 46.41; H, 4.03; N, 9.83.

Syntheses of [(Am2Py3)Ni(NCCH₃)](BF₄)₂ (2a**).** Compound **2a** was prepared with an essentially identical protocol as that adopted for the preparation of **1a** but using **Am2Py3** (0.43 g, 1.0 mmol) as ligand. The product was obtained as rod-shaped amaranthine crystals in a yield of 75% (0.52 g). ¹H NMR (400 MHz, CD₃COCD₃): δ 2.01, 5.71, 7.62, 9.02, 14.19, 15.04, 45.91, and 47.45. TOF-MS: Calcd for [M–CH₃CN–BF₄]⁺ (C₂₇H₂₉BN₅F₄Ni): *m/z* 568.1806; found: 568.1809. Anal. Calcd for C₂₉H₃₂N₆B₂F₈Ni (%): C, 49.98; H, 4.63; N, 12.06; found: C, 49.85; H, 4.61; N, 12.02.

Syntheses of [(Am2Py3)Ni(H₂O)](BF₄)₂ (2b**).** Compound **2b** was prepared with a similar protocol as that adopted for the preparation of **2a** but using water as solvent. The product was obtained as amaranthine crystals in a yield of 83% (0.56 g). ¹H NMR (400 MHz, CD₃COCD₃): δ 2.05, 3.01, 5.71, 7.51, 8.98, 14.07, 14.85, 14.98, 44.67, and 44.83. TOF-MS: Calcd for

$[M-BF_4-H_2O]^+$ ($C_{27}H_{29}N_5BF_4Ni$): m/z 568.1806; found: 568.1807. Anal. Calcd for $C_{27}H_{31}N_5OB_2F_8Ni \cdot 2H_2O$ (%): C, 45.68; H, 4.97; N, 9.87; found: C 45.63, H 4.95, N 9.90.

Syntheses of $[(Am_3Py_2)Ni(NCCH_3)](BF_4)_2$ (3a**).** The preparation of **3a** was made in a similar way as that adopted for the preparation of **1a** but using Am_3Py_2 (0.56 g, 1.0 mmol) as ligand. The product was obtained as blue-green crystals in a yield of 75% (0.62 g). 1H NMR (400 MHz, CD_3COCD_3): δ 0.43, 5.95, 6.05, 6.48, 7.12, 8.71, 8.93, 9.26, 9.53, 9.92, 10.31, 11.18, 14.74, 14.95, 17.94, 32.73, 42.43, 47.32, and 54.73. TOF-MS: Calcd for $[M-BF_4-NCCH_3]^+$ ($C_{37}H_{41}N_5BF_4Ni$): m/z 700.2745; found: 700.2741. Anal. Calcd for $C_{39}H_{44}N_6B_2F_8Ni$ (%): C, 56.50; H, 5.35; N, 10.14; found: C, 56.42; H, 5.30; N, 10.01.

Syntheses of $[(Am_3Py_2)Ni(OH_2)](BF_4)_2$ (3b**).** The preparation of **3b** was made in a similar way as that adopted for the preparation of **3a** but using water as solvent. The product was obtained as blue-green crystals in a yield of 79% (0.64 g). 1H NMR (400 MHz, CD_3COCD_3): δ 2.11, 5.62, 6.04, 6.50, 7.14, 8.70, 8.99, 9.26, 9.52, 9.96, 10.42, 11.22, 14.71, 14.95, 18.08, 32.39, 42.67, 47.33, and 54.67. TOF-MS: Calcd for $[M-BF_4-NCCH_3]^+$ ($C_{37}H_{41}N_5BF_4Ni$): m/z 700.2745; found: 700.2747. Anal. Calcd for $C_{37}H_{43}N_5OB_2F_8Ni$ (%): C, 55.13; H, 5.38; N, 8.69; found: C, 55.07; H, 5.41; N, 8.53.

Crystallographic structure determinations

The single-crystal X-ray diffraction data were collected with an Bruker Smart Apex II CCD diffractometer with a graphite-monochromated $Mo-K_\alpha$ radiation ($\lambda = 0.071073 \text{ \AA}$) at 296 K using the ω - 2θ scan mode. Data processing was accomplished with the SAINT processing program.^{S7} Intensity data were corrected for absorption by the SADABS program.^{S8} All structures were solved by direct methods and refined on F^2 against full-matrix least-squares methods by using the SHELXTL 97 program package.^{S9} All non-hydrogen atoms were refined anisotropically. Hydrogen atoms were located by geometrical calculation.

Crystallographic data and selected bond lengths and angles for **1a–3a** and **2b** are given in Tables S1–S3. Molecular structures of **1a–3a** and **2b** are given in Figs. 2 and S8. CCDC-989005 (**1a**), -989006 (**2a**), -989008 (**3a**), and -989007 (**2b**), contain the supplementary crystallographic data for this paper. These data can be obtained free of charge from The Cambridge Crystallographic Data Centre via www.ccdc.cam.ac.uk/data_request/cif.

Electrochemistry studies

CV measurements in THF or CH₃CN. Cyclic voltammetry experiments were carried out in a three-electrode cell under Ar using CHI650E potentiostat. The working electrode was a glassy carbon disc (diameter 3 mm) polished with 3 and 1 μm diamond pastes and sonicated in ion-free water for 15 min prior to use. The reference electrode was a non-aqueous Ag/AgNO₃ (0.01 M AgNO₃ in CH₃CN) electrode and the counter electrode was platinum wire. A solution of 0.1 M *n*Bu₄NPF₆ (Fluka, electrochemical grade) in THF or CH₃CN was used as supporting electrolyte, which was degassed by bubbling with dry argon for 15 min before measurement. The ferricinium/ferrocene (Fc⁺⁰) couple was used as an internal reference and all potentials given in this work are referred to the Fc⁺⁰ potential ($E(\text{Fc}^{+/0}) = 0.64 \text{ V vs. SHE}$).

Theoretically, two important criteria, $\Delta E_p = E_{pa} - E_{pc} = 59/n \text{ mV}$ and $|I_{pa}/I_{pc}| = 1$,^{S10} are used to diagnose a reversible redox wave. Here E_{pa} is the peak potential for anodic process (V); E_{pc} is the peak potential for cathodic process (V); I_{pa} is the peak current for anodic process (A cm^{-2}); and I_{pc} is the peak current for cathodic process (A cm^{-2}). In practice, some experimental conditions may influence the ΔE_p value. Considering the influence of experimental conditions, we added ferrocene as an internal reference as the Fc^{+/0} wave is known as a one-electron reversible redox process. The ΔE_p values of the first reduction waves of **2b**, **3b**, **2a**, and **3a** in their CVs (Figs. 3b, 3c and Figs. S12b, S12c) are all similar to the

ΔE_p value measured for the Fc^+/Fc ; and the $|I_{pa}/I_{pc}|$ values of the first reduction waves of these four nickel complexes are in the range of 0.93 to 0.97. Therefore the first reduction waves of **2b**, **3b**, **2a**, and **3a** are diagnosed as reversible waves. In contrast, the first reduction waves of **1a** and **1b**, and the second reduction events of all nickel complexes are irreversible reduction events as these waves have no reverse peak or have a very small reverse peak.

CV measurements in water. The cyclic voltammograms were recorded on a PGSTAT100N potentiostat with a controlled-growth mercury electrode (drop size $\sim 0.4 \text{ mm}^2$), a platinum wire auxiliary electrode, and an aqueous Ag/AgCl reference electrode. The solution was stirred constantly during controlled potential electrolysis experiments.

Controlled potential electrolysis experiments (CPE) in water. All CPE experiments made in water were carried out in a pear-shaped double-compartment cell except for measurements of Faradaic efficiency. A mercury pool with a surface area of 3.1 cm^2 was used as the working electrode for electrochemical studies conducted in aqueous media. Electrical contact of the mercury pool was achieved through a platinum wire immersed below the surface of the mercury. The auxiliary electrode, a 4 cm^2 platinum gauze, was placed in a column-shaped compartment with a bottom of porous glass frit (G3, 1.1 cm^2), which was inserted into the main chamber of the electrolysis experiment and fixed only $\sim 1 \text{ cm}$ above the surface of mercury pool electrode to reduce the internal resistance. The sample was bubbled with argon for 20 min before measurement and the electrolysis was carried out under Ar. The solutions in both compartments were constantly stirred during electrolysis experiments. The reference electrode was a commercially available aqueous Ag/AgCl electrode and the potentials were reported with respect to SHE by adding 0.195 V to the experimentally measured values.

Bulk electrolysis. The controlled potential electrolysis experiments were conducted in a cell with the working electrode compartment containing 20–40 mL of 2.0 M phosphate buffer

solution at pH 7 and the counter electrode compartment containing 5–10 mL of the same buffer used in the working electrode compartment. The volume of the gas generated during electrolysis experiment was quantified by a gas burette and the H₂ content was determined by GC analysis using a GC 7890T instrument with a thermal conductivity detector, a 5 Å molecular sieve column (2 mm × 5 m) and with N₂ as carrying gas. Each catalytic datum was obtained from at least two paralleled experiments.

Determination of Faradaic Efficiency. Gas chromatographic analysis of the electrolysis-cell headspace was made during the electrolysis of a solution of 5 μM **2b** in 30 mL of 2.0 M phosphate buffer at pH 7 in a gas-tight electrolysis cell at an applied potential of –1.25 V vs. SHE for 1 h with a mercury pool electrode (surface area 3.1 cm²). The amount of hydrogen generated was determined by the external standard method and the hydrogen dissolved in the solution was neglected. The Faradaic efficiency of ~91% was calculated by the equation: (the moles of H₂ evolved during the CPE process) / (the moles of H₂ calculated based on consumed charges) × 100% (Fig. S20).

References

- S1 P. Zhang, M. Wang, F. Gloaguen, L. Chen, F. Quentelb and L. Sun, *Chem. Commun.*, 2013, **49**, 9455.
- S2 N. Ortega-Villar, V. M. Ugalde-Saldivar, M. C. Munoz, L. A. Ortiz-Frade, J. G. Alvarado-Rodriguez, J. A. Real and R. Moreno-Esparza, *Inorg. Chem.*, 2007, **46**, 7285.
- S3 (a) L. Duelund, R. Hazell, C. J. McKenzie, L. P. Nielsen and H. Toftlund, *J. Chem. Soc., Dalton Trans.*, 2001, 152; (b) M. V. de Almeida, A. P. S. Fontes, R. N. Berg, E. T. Cesar, E. de C. A. Felicio and J. D. de S. Filho, *Molecules* 2002, **7**, 405.
- S4 (a) G. Roelfes, M. E. Branum, L. Wang, L. Que and B. L. Feringa, *J. Am. Chem. Soc.*, 2000, **122**, 11517; (b) C. Jubert, A. Mohamadou, J. Marrot and J.-P. Barbier, *J. Chem. Soc.*,

- Dalton Trans.*, 2001, 1230.
- S5 M. S. Vad, A. Nielsen, A. Lennartson, A. D. Bond, J. E. McGrady and C. J. McKenzie, *Dalton Trans.*, 2011, **40**, 10698.
- S6 G. Roelfes, M. Lubben, K. Chen, R. Y. Ho, A. Meetsma, S. Genseberger, R. M. Hermant, Hage R, S. K. Mandal, V. G. Young, Y. Zang, H. Kooijman, A. L. Spek, L. Que and B. L. Feringa, *Inorg. Chem.*, 1999, **38**, 1929.
- S7 G. M. Sheldrick, SHELXTL97 Program for the Refinement of Crystal Structure, University of Göttingen, Germany, 1997.
- S8 Software packages SMART and SAINT, Siemens Energy & Automation Inc., Madison, Wisconsin, 1996.
- S9 G. M. Sheldrick, SADABS Absorption Correction Program, University of Göttingen, Germany, 1996.
- S10 R. Greef, R. Peat, L. M. Peter, D. Pletcher, J. Robinson, *Instrumental methods in electrochemistry*, Southampton electrochemistry group, Ellis Horwood Limited, 1985, England.

Table S1 Crystallographic data and processing parameters for **1a–3a** and **2b**

Complex	1a	2a	3a	2b
Formula	C ₂₅ H ₂₄ N ₆ NiB ₂ F ₈	C ₂₉ H ₃₂ N ₆ NiB ₂ F ₈	C ₄₃ H ₅₀ N ₉ NiB ₂ F ₈	C ₂₇ H ₃₃ N ₅ NiO ₂ B ₂ F ₈
Formula weight	640.80	696.91	911.21	687.88
Crystal system	monoclinic	monoclinic	monoclinic	orthorhombic
Space group	P-62c	P2(1)/n	P2(1)/c	Pbcn
Z	6	4	4	8
a / Å	18.058(4)	11.0812(5)	10.3663(12)	10.5139(12)
b / Å	18.058(4)	23.7229(11)	28.640(4)	14.6832(17)
c / Å	14.612(3)	13.0438(6)	16.685(2)	40.182(5)
α / deg	90.00	90.00	90.00	90.00
β / deg	90.00	113.471(2)	107.340(7)	90.00
γ / deg	120.00	90.00	90.00	90.00
V / Å ³	4126.5(15)	3145.2(2)	4728.5(10)	6203.3(12)
D _{calcd} / g m ⁻³	1.555	1.465	1.274	1.473
μ / mm ⁻¹	0.790	0.695	0.480	0.708
Crystal size / mm	0.21×0.15×0.16	0.30×0.16×0.13	0.27×0.14×0.15	0.24×0.17×0.12
θ Range / deg	1.30 / 28.42	1.91 / 25.00	1.91 / 27.68	2.03 / 27.51
Reflns collected / Indep.	25339/3587	12472/5536	30791/10980	39721/7120
Parameters refined	206	415	534	406
F(000)	1956	1420	1880	2816
GOF on F ²	1.023	1.102	1.119	1.023
Final R ₁ (I > 2σ(I))	0.0699	0.0682	0.1197	0.0677
Final wR ₂ (I > 2σ(I))	0.1700	0.2118	0.3284	0.1906
max. peak/hole / e Å ⁻³	0.900, -0.370	0.805, -0.616	0.831, -0.715	0.813, -0.522

$$R_1 = \frac{\sum ||F_o| - |F_c||}{\sum |F_o|}, wR_2 = \left[\frac{\sum (|F_o|^2 - |F_c|^2)^2}{\sum (F_o^2)} \right]^{1/2}$$

Table S2 Selected bond lengths (Å) and angles (deg) for **1a–3a**

Complex	1a	2a	3a
Bond lengths			
Ni–N1	2.086(4)	2.096(3)	2.127(5)
Ni–N2	2.086(4)	2.076(3)	2.207(5)
Ni–N3	2.063(5)	2.104(4)	2.068(5)
Ni–N4	2.080(4)	2.147(3)	2.115(5)
Ni–N5	2.080(4)	2.149(3)	2.111(6)
Ni–N6	2.027(6)	2.064(3)	2.250(5)
Bond angles			
N1–Ni–N2	84.2(2)	97.62(13)	83.91(18)
N1–Ni–N3	80.37(15)	80.32(15)	158.3(2)
N1–Ni–N4	93.62(15)	95.74(12)	101.3(2)
N1–Ni–N5	162.59(15)	172.91(12)	96.2(2)
N1–Ni–N6	96.85(17)	90.35(13)	82.36(18)
N2–Ni–N3	80.37(15)	78.89(15)	78.2(2)
N2–Ni–N4	162.59(15)	156.44(13)	173.6(2)
N2–Ni–N5	93.62(15)	89.35(13)	89.0(2)
N2–Ni–N6	96.85(17)	100.36(14)	107.96(18)
N3–Ni–N4	82.24(14)	84.36(14)	97.5(2)
N3–Ni–N5	82.23(14)	102.44(15)	95.6(2)
N3–Ni–N6	176.2(2)	170.42(15)	91.47(19)
N4–Ni–N5	83.3(2)	78.16(12)	86.8(2)
N4–Ni–N6	100.56(17)	98.87(13)	76.7(2)
N5–Ni–N6	100.56(17)	87.08(13)	162.7(2)

Table S3 Selected bond lengths (Å) and angles (deg) for **2b**

Complex	2b
Bond lengths	
Ni–O1	2.073(3)
Ni–N1	2.077(3)
Ni–N2	2.102(3)
Ni–N3	2.100(3)
Ni–N4	2.175(3)
Ni–N5	2.079(3)
Bond angles	
O1–Ni–N1	93.38(12)
O1–Ni–N2	175.39(12)
O1–Ni–N3	99.07(13)
O1–Ni–N4	96.71(11)
O1–Ni–N5	88.93(12)
N1–Ni–N2	82.12(13)
N1–Ni–N3	89.38(12)
N1–Ni–N4	95.71(12)
N1–Ni–N5	176.02(12)
N2–Ni–N3	79.91(13)
N2–Ni–N4	84.83(11)
N2–Ni–N5	95.61(13)
N3–Ni–N4	163.10(12)
N3–Ni–N5	93.45(12)
N4–Ni–N5	80.80(12)

Table S4 The redoxpotentials of **1a–3a** and **1b–3b** in 0.1 M *n*Bu₄NPF₆/THF

Catalyst	N _{amine} : N _{pyridine}	<i>E</i> _{pc1} V vs SHE	<i>E</i> _{pc2} V vs SHE	$\Delta E(E_{pc1} - E_{pc2})$ V
1a	1 : 4	-1.33	-2.07	0.74
2a	2 : 3	-1.12	-1.89	0.77
3a	3 : 2	-0.85	-2.05	1.20
1b	1 : 4	-1.35	-2.06	0.71
2b	2 : 3	-1.03	-1.95	0.92
3b	3 : 2	-0.87	-2.10	1.23

Table S5 The onsetpotentials of **1b–3b** in neutral phosphate buffer

Catalyst	N _{amine} : N _{pyridine}	<i>E</i> _{onset} V vs SHE
1b	1 : 4	-1.10
2b	2 : 3	-1.13
3b	3 : 2	-1.22

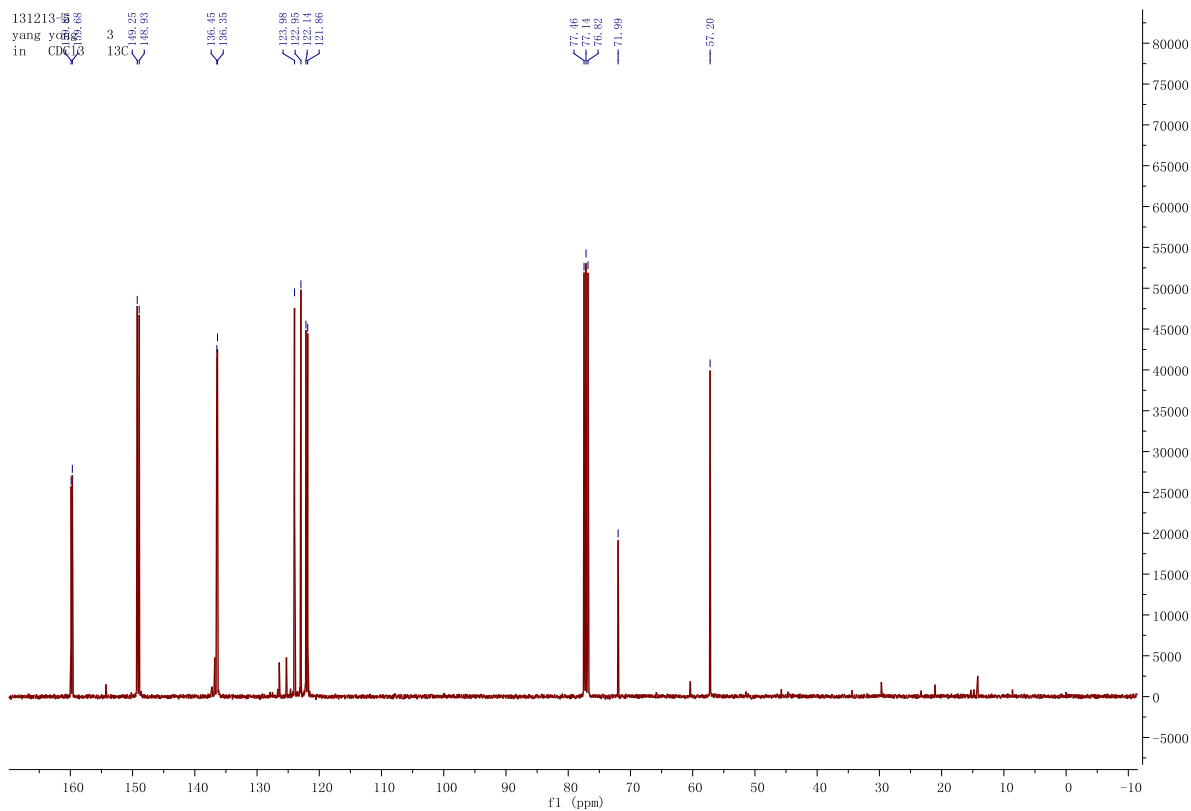
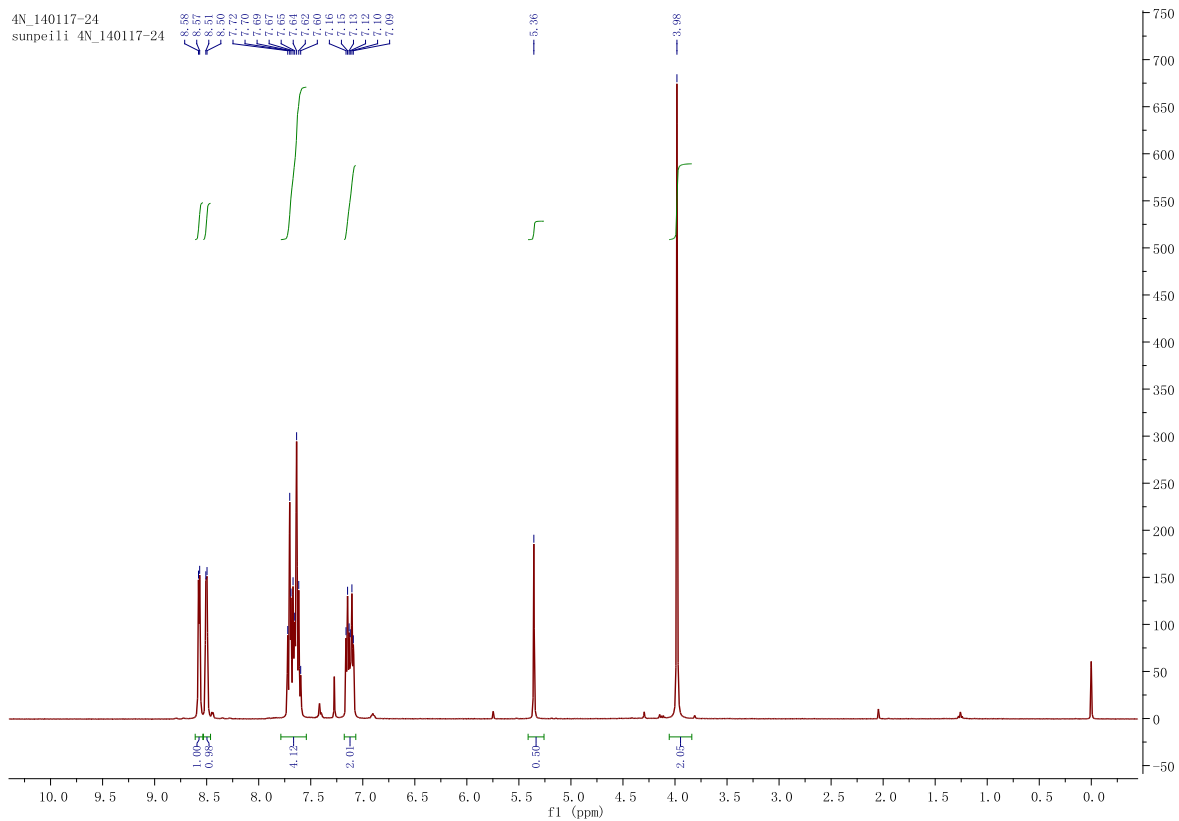


Fig. S1 (top) ^1H and (bottom) ^{13}C NMR spectra of ligand **Am1Py4** in CDCl_3 .

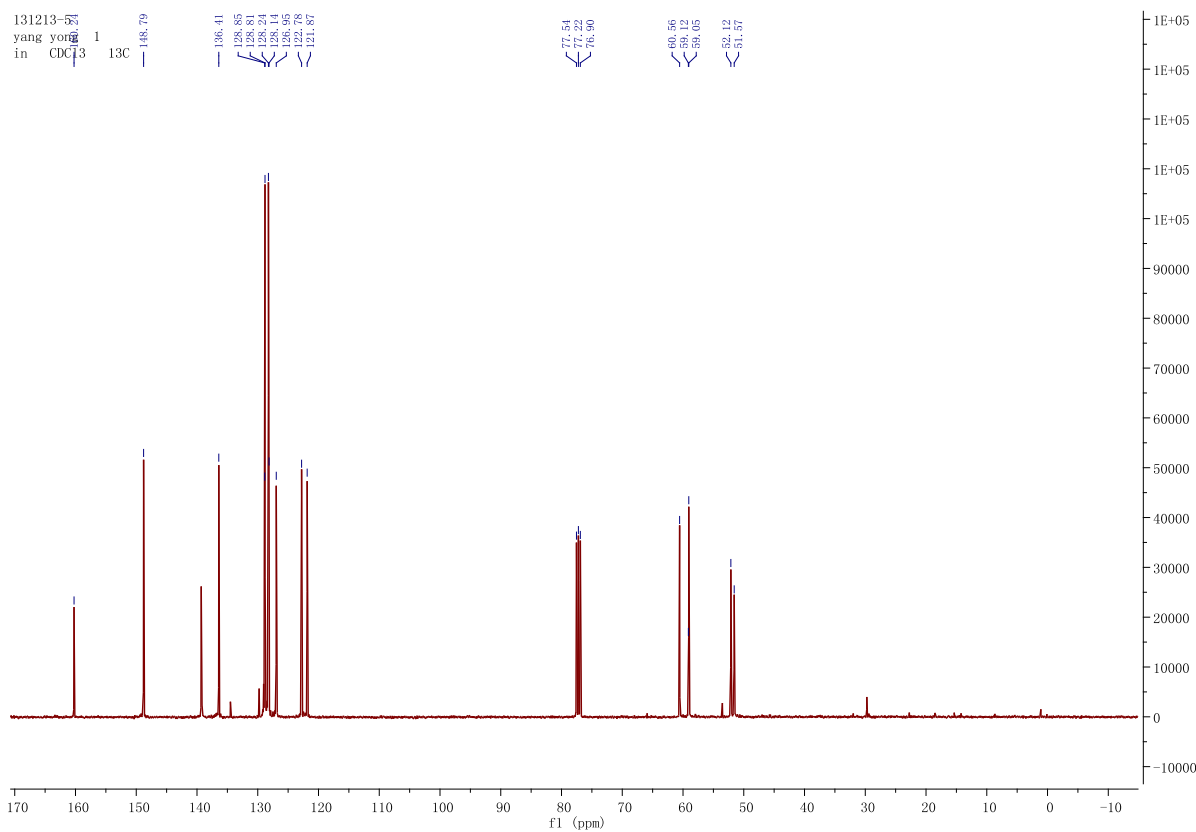
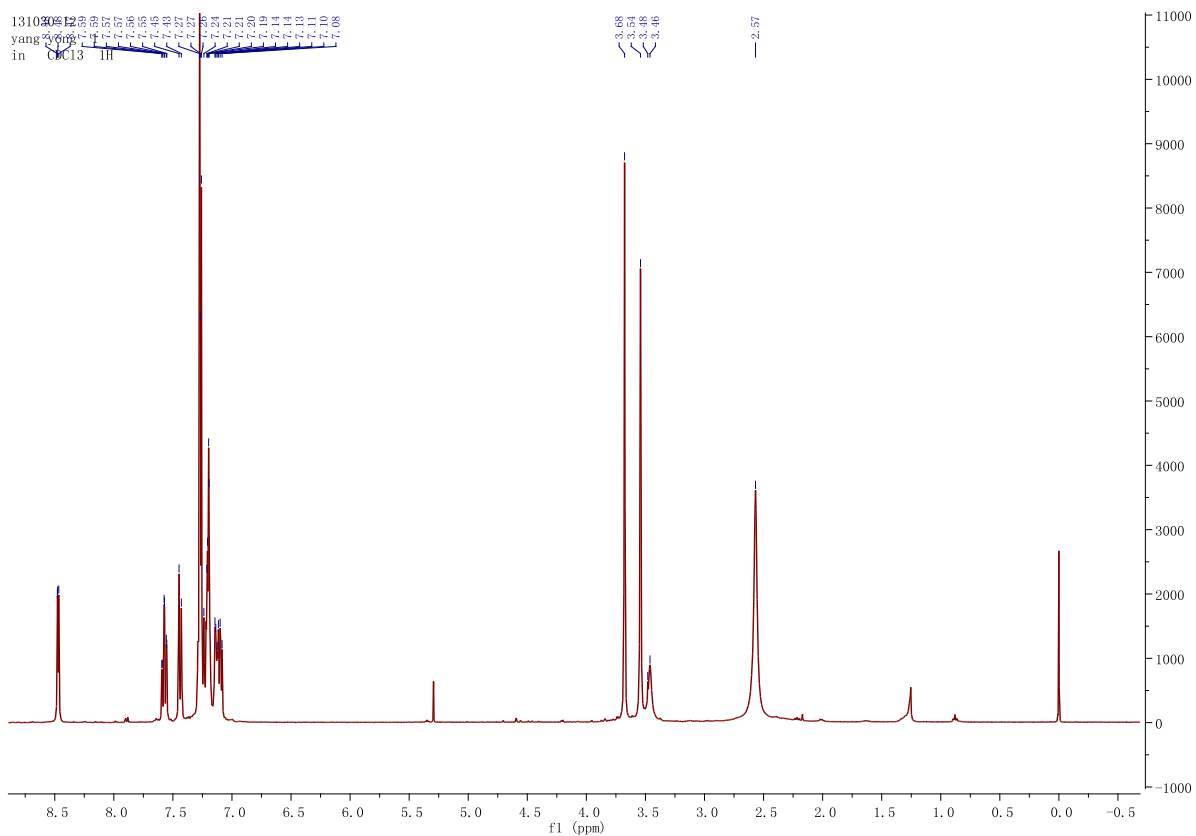
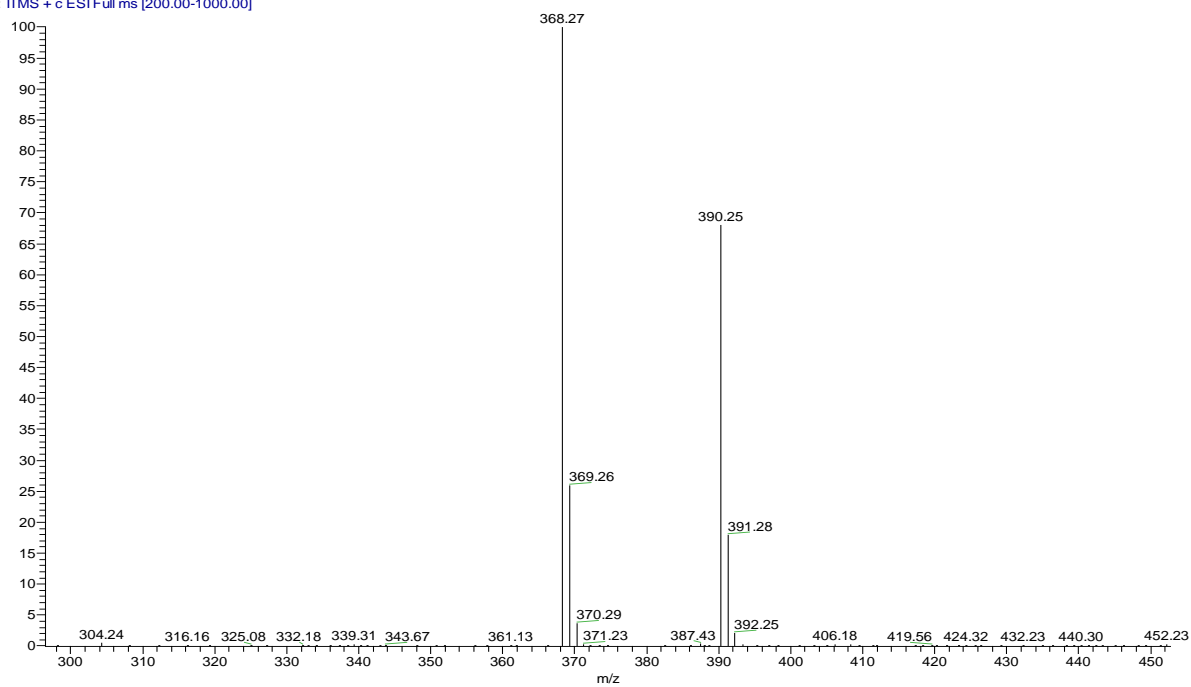


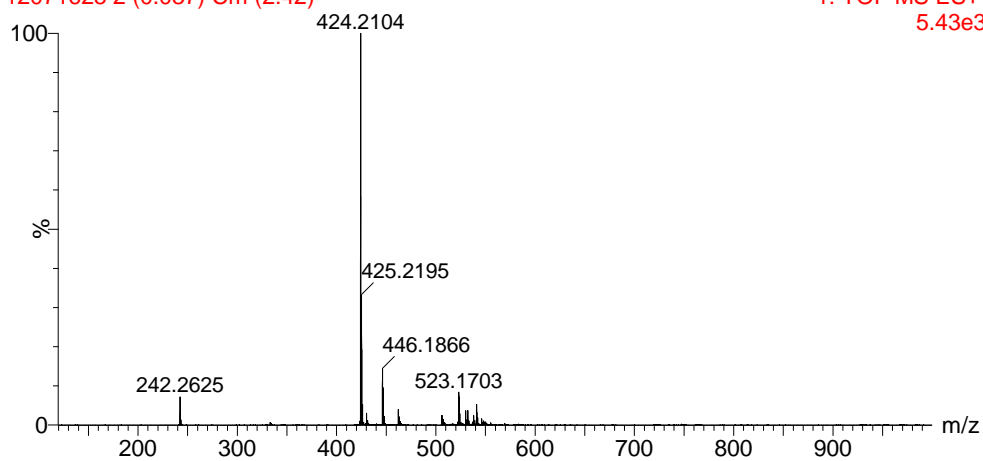
Fig. S3 (top) ¹H and (bottom) ¹³C NMR spectra of ligand **Am3Py2** in CDCl₃.

YY-M367 #30-35 RT: 0.07-0.08 AV: 6 SB: 25 0.88-0.93 NL: 2.50E5
T: ITMS + c ESI Full ms [200.00-1000.00]



12071625 2 (0.037) Cm (2:42)

1: TOF MS ES+
5.43e3



14091213 23 (0.426) AM (Cen,2, 80.00, Ht,5000.0,0.00,1.00); Sm (SG, 2x3.00); Cm (13:23)

1.79e4

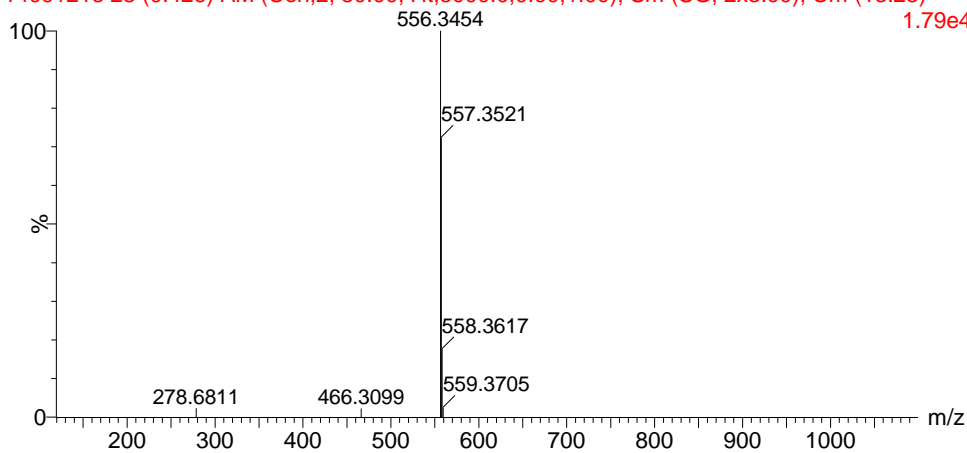
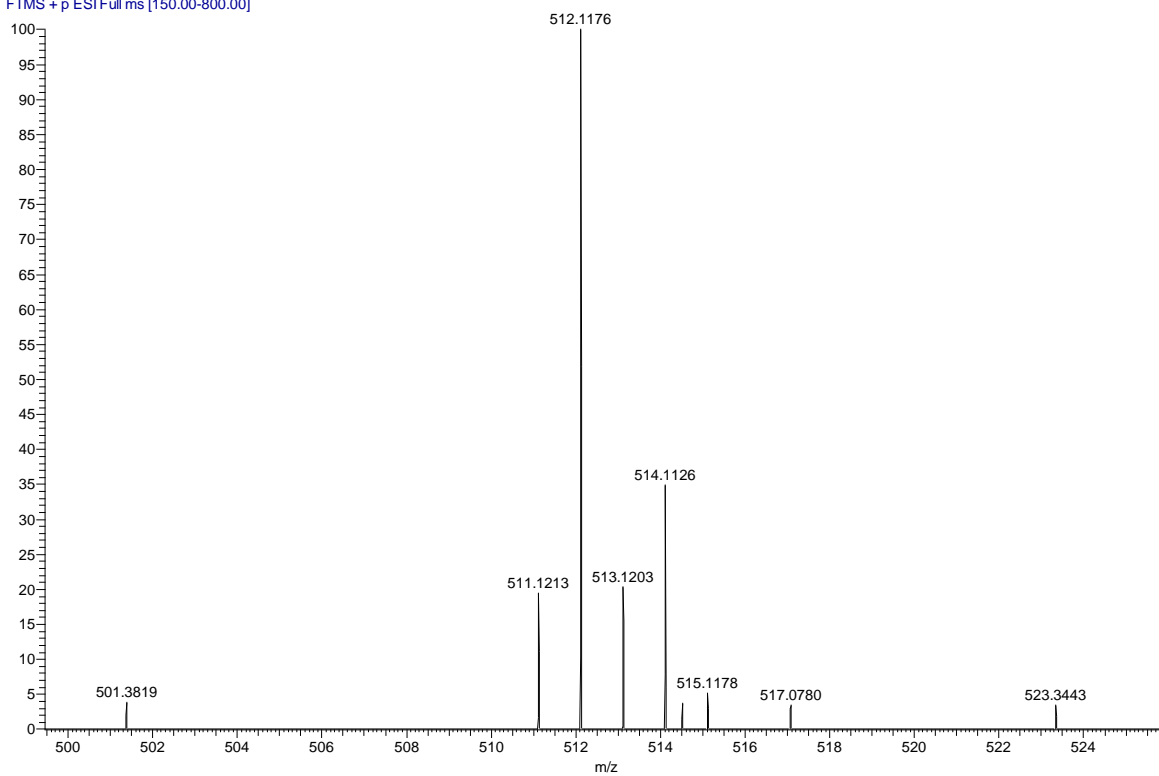


Fig. S4 Mass spectra of ligands (top) **Am1Py4**, (middle) **Am2Py3**, and (bottom) **Am3Py2**.

YY1-NL_131219154724 #14-15 RT: 0.10-0.11 AV: 2 SB: 8 0.88-0.93 NL: 3.59E5
T: FTMS + p ESI Full ms [150.00-800.00]



yy2-ni #14-17 RT: 0.10-0.12 AV: 4 SB: 7 0.92-0.97 NL: 5.50E5
T: FTMS + p ESI Full ms [150.00-1000.00]

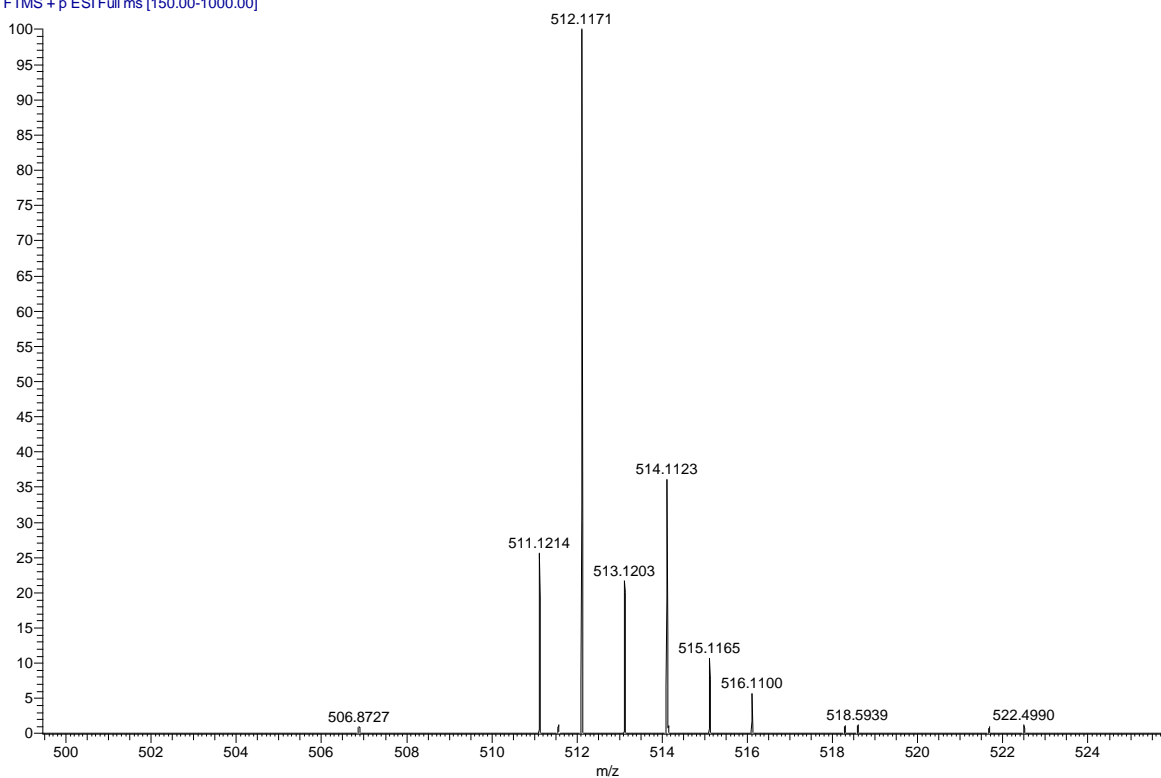


Fig. S5 Mass spectra of nickel complexes (top) **1a** and (bottom) **1b**.

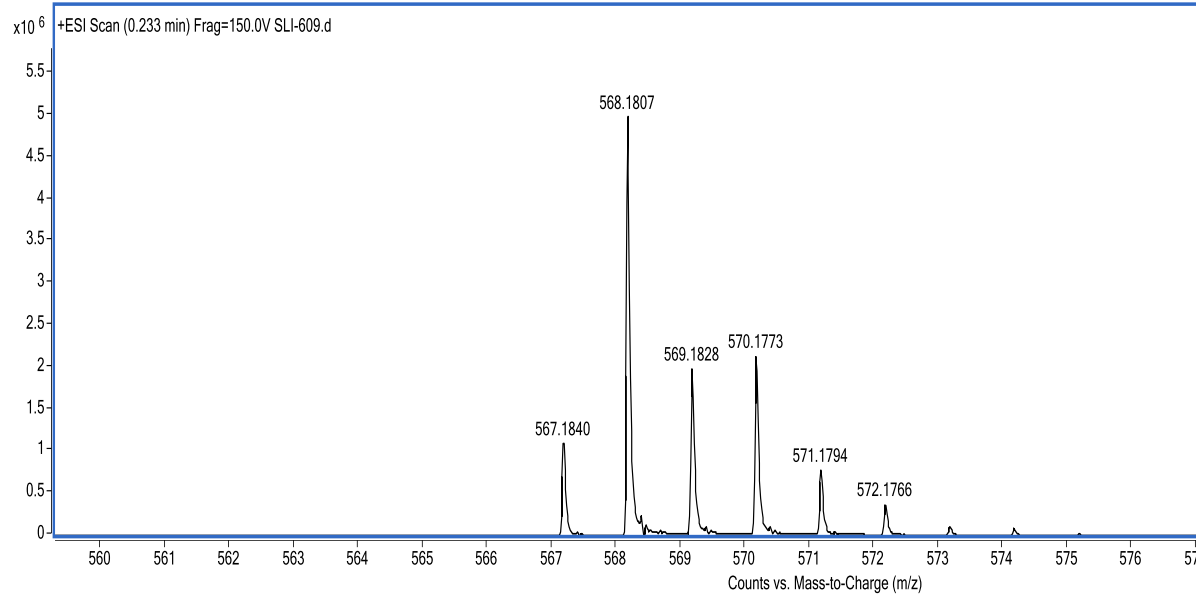
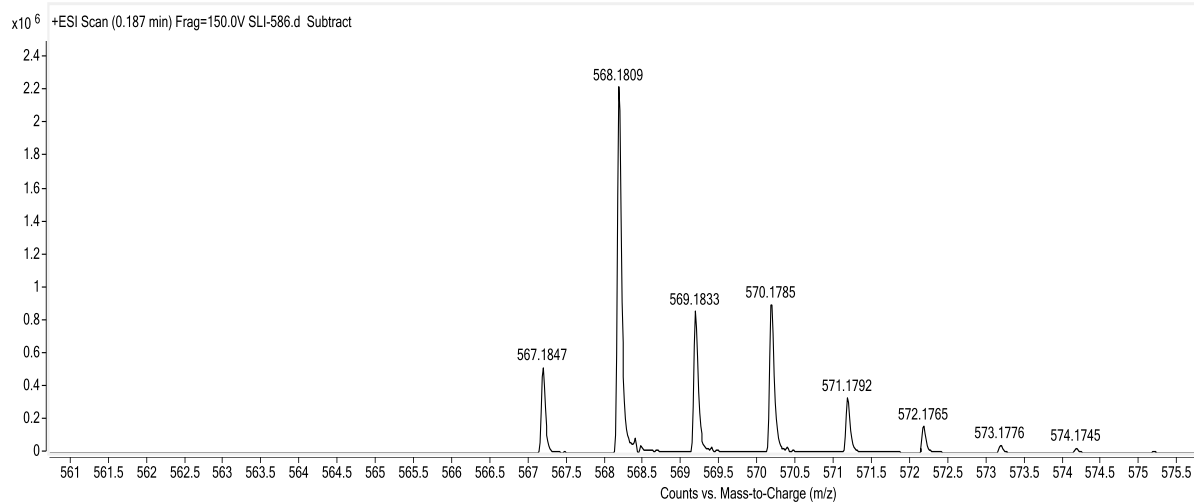
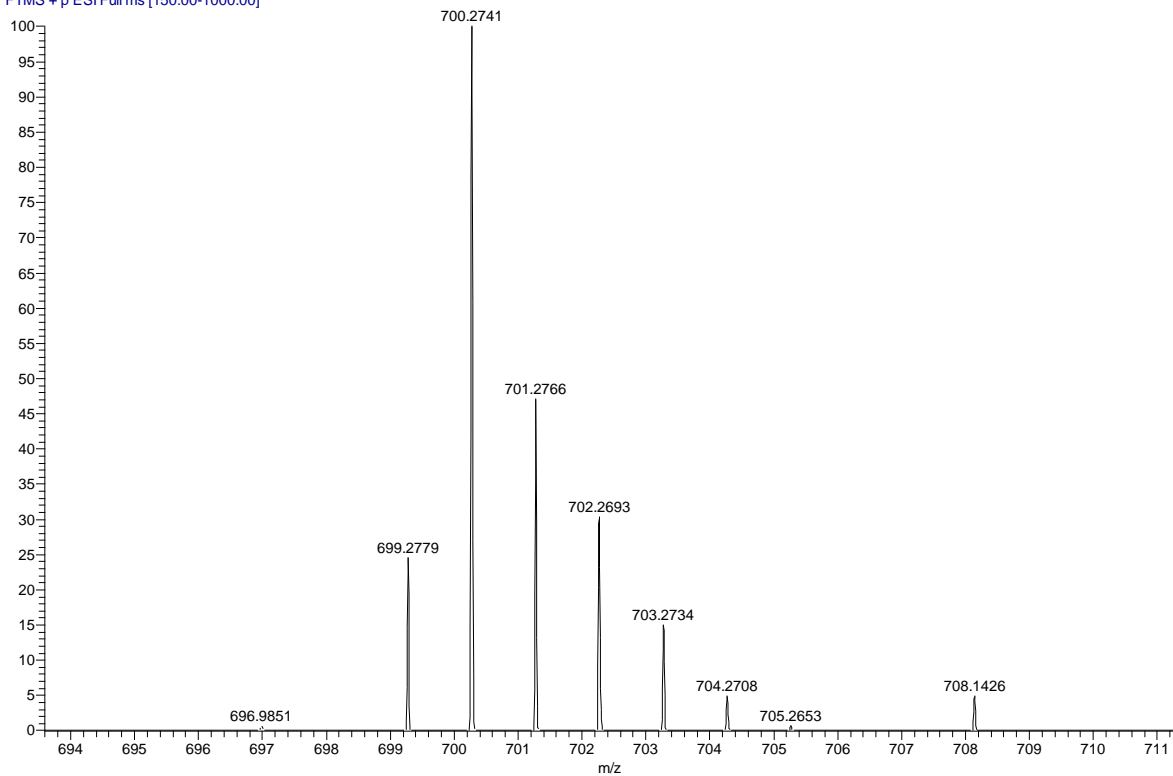


Fig. S6 Mass spectra of nickel complexes (top) **2a** and (bottom) **2b**.

w3-ni #13-16 RT: 0.09-0.12 AV: 4 SB: 8 0.88-0.93 NL: 9.32E5
T: FTMS + p ESI Full ms [150.00-1000.00]



yy4-ni #14-19 RT: 0.10-0.14 AV: 6 SB: 7 0.86-0.91 NL: 3.75E5
T: FTMS + p ESI Full ms [150.00-1000.00]

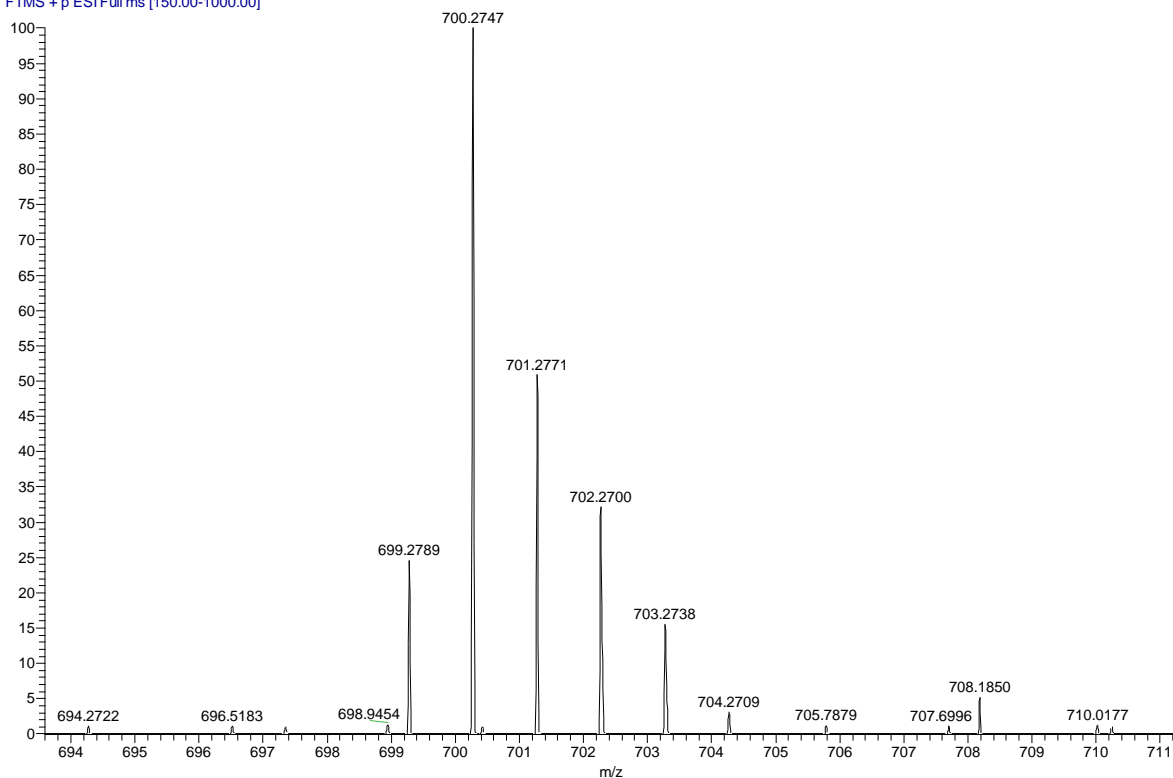


Fig. S7 Mass spectra of nickel complexes (top) **3a** and (bottom) **3b**.

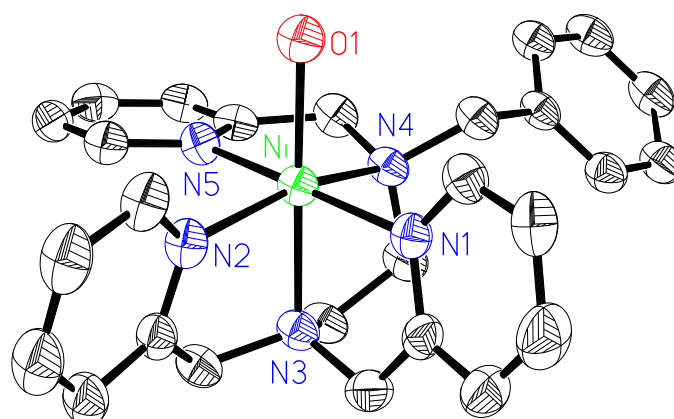


Fig. S8 Molecular structures of **2b** with thermal ellipsoids shown at 30% probability.

Counterions, solvent molecules and hydrogen atoms are omitted for clarity.

To see whether there is a ligand (H_2O or CH_3CN) exchange when these nickel complexes are dissolved in THF, **2a** and **2b** were dissolved and recrystallized in THF, respectively. The corresponding crystals obtained from THF are named as **2a'** and **2b'**. The absorption at 2288 cm^{-1} in the Raman spectrum (Figure S9) of **2a** (crystallized from CH_3CN) is attributed to the coordinating molecule of CH_3CN . The crystal **2a'** obtained from THF displays an exactly identical absorption as **2a**, indicating that the apical CH_3CN is still in the complex after recrystallized in THF. Furthermore, the crystal structures of **2a'** (Figure S10) and **2b'** (Figure S11) confirm that the apical CH_3CN and H_2O ligands cannot be substituted by the molecule of solvent, THF. Figure S11 shows that **2b'** still possesses the apical H_2O when dissolved and recrystallized in THF. In the crystal cell of **2b'**, there is a free THF molecule, which does not replace the apical H_2O in **2b'**.

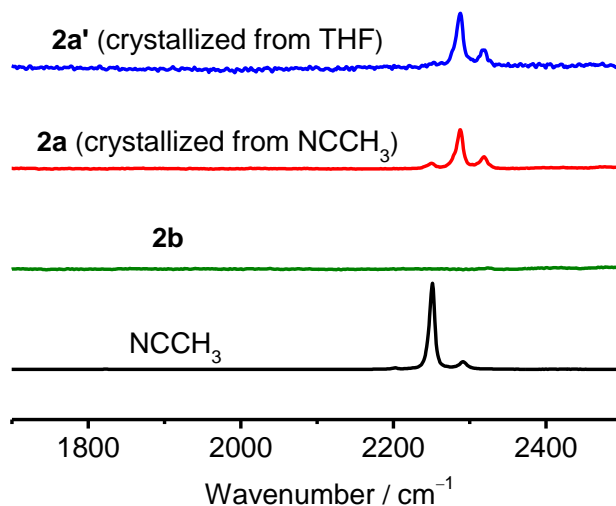


Fig. S9 Raman spectra of **2a'** (blue, crystallized from THF), **2a** (red, crystallized from CH_3CN), **2b** (green) and CH_3CN (black).

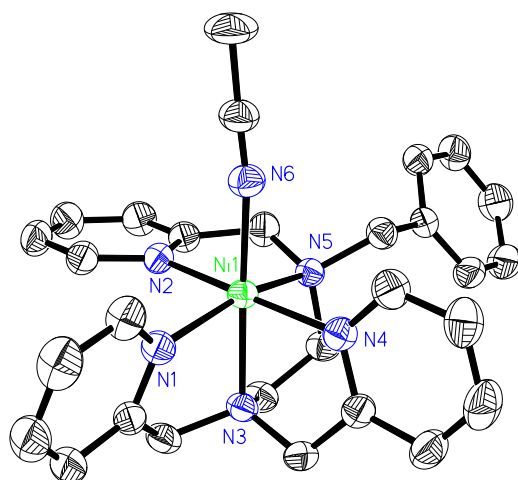


Fig. S10 Crystal structure of **2a'** crystallized from THF, with thermal ellipsoids shown at 30% probability. Counterions and hydrogen atoms are omitted for clarity.

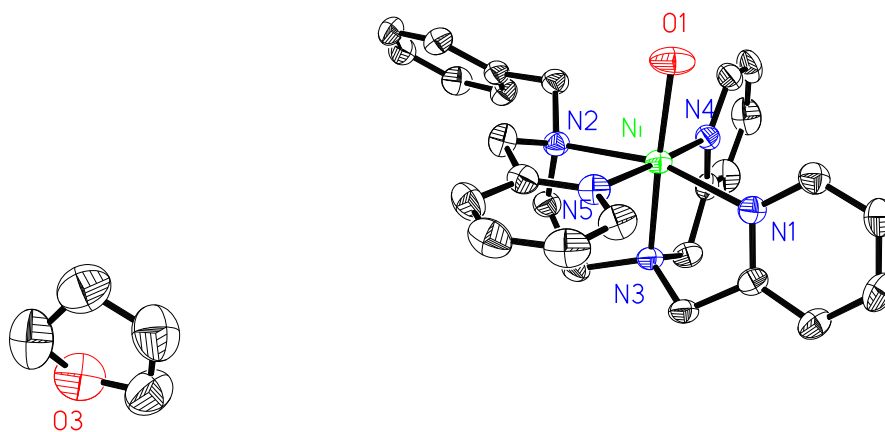


Fig. S11 Crystal structure of **2b'** crystallized from THF, with thermal ellipsoids shown at 30% probability. Counterions and hydrogen atoms are omitted for clarity.

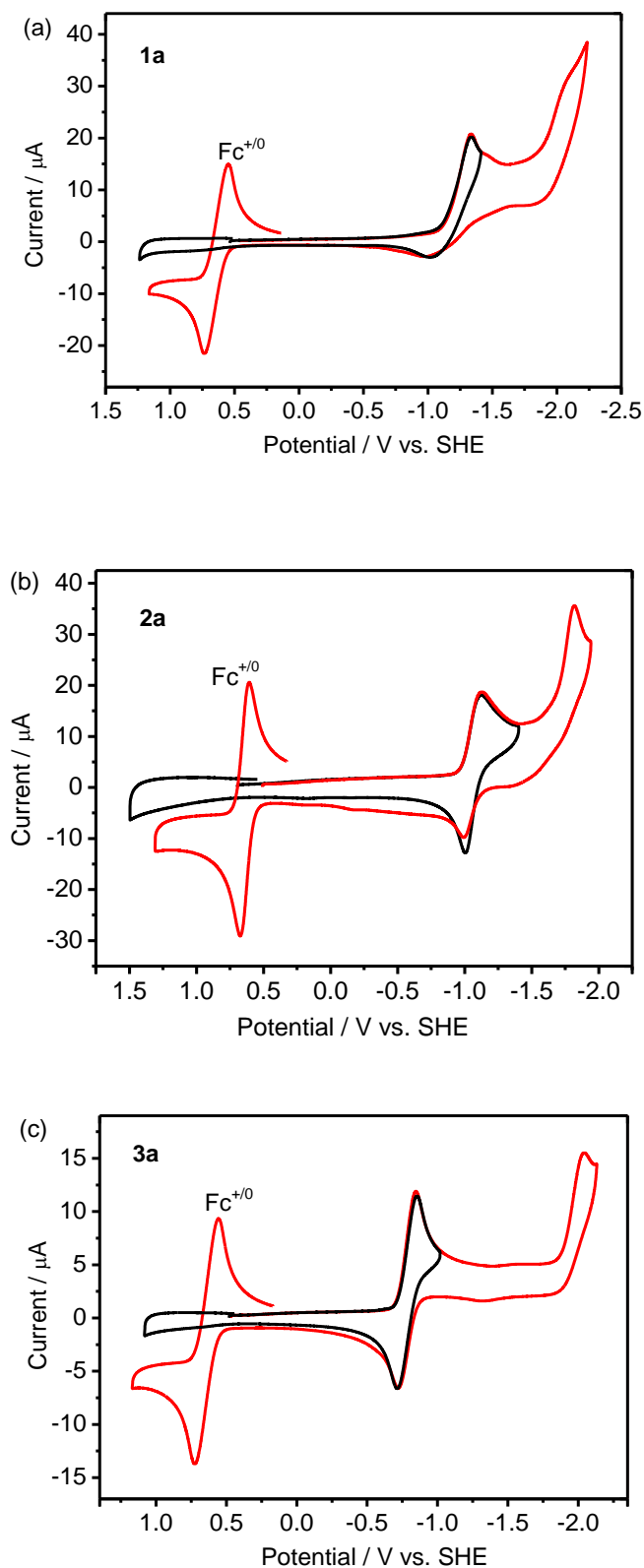


Fig. S12 Cyclic voltammograms of **1a**, **2a** and **3a** in 0.1 M $n\text{Bu}_4\text{NPF}_6/\text{THF}$ with (red) and without (black) the internal reference ($E(\text{Fc}^{+/0}) = 0.64$ V vs. SHE), scan rate 100 mV s^{-1} .

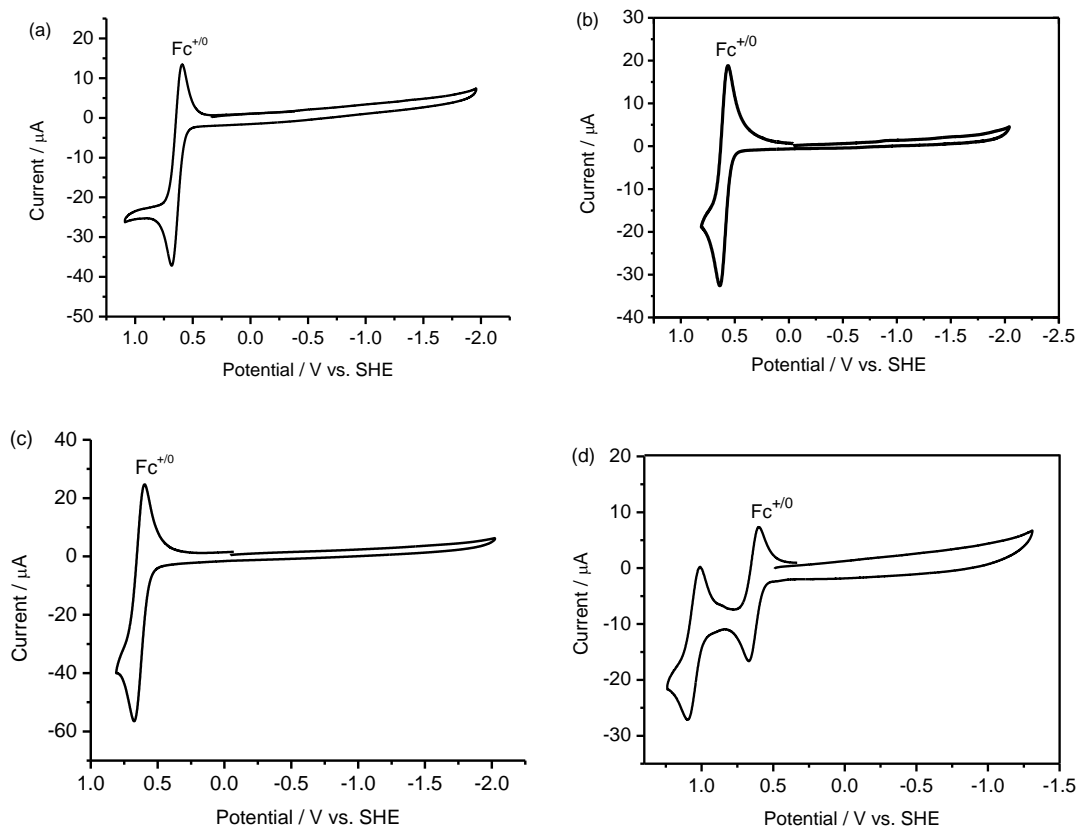


Fig. S13 Cyclic voltammograms of 1.0 mM (a) **Am1Py4**, (b) **Am2Py3**, (c) **Am3Py2**, and (d) $[\text{Fe}(\text{Am2Py3})(\text{CH}_3\text{CN})]^{2+}$ (**4**) in 0.1 M $n\text{Bu}_4\text{NPF}_6/\text{CH}_3\text{CN}$ with the internal reference ($E(\text{Fc}^{+/0}) = 0.64$ V vs. SHE), scan rate 100 mV s^{-1} .

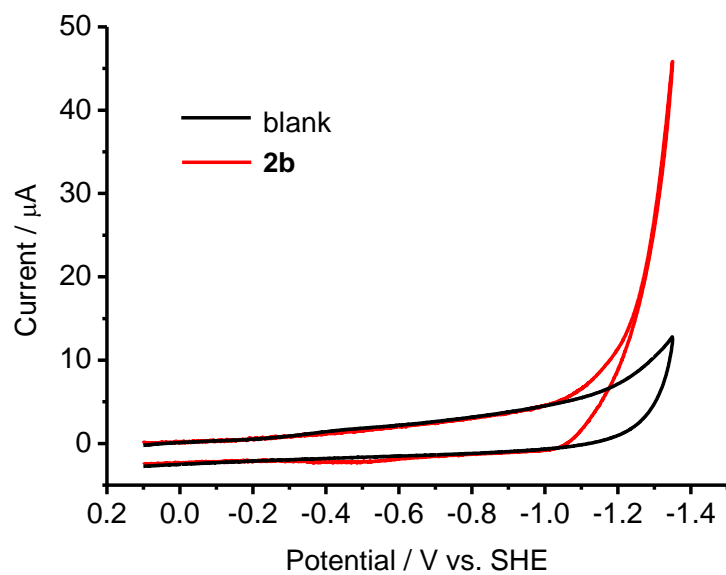


Fig. S14 Cyclic voltammograms of 2.0 M phosphate buffer at pH 7 with 0.1 M **2b** (red) and without catalyst (black) using a glassy carbon as working electrode (7 mm²).

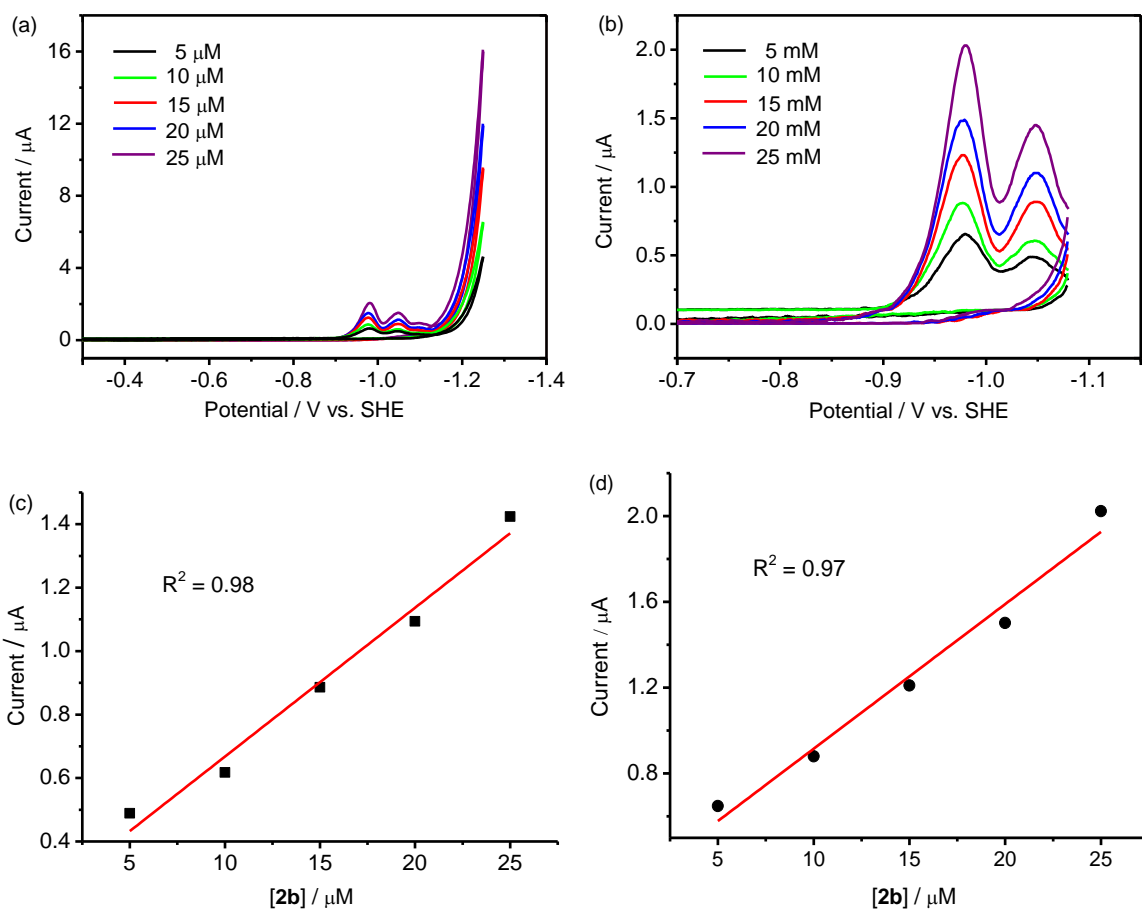


Fig. S15 Cyclic voltammograms of (a) **2b** in 1.0 M phosphate buffer at pH 7 with a controlled growth mercury drop electrode; (b) a selected region from (a) for the first and second peaks; Plots of (c) the first and (d) the second reduction current versus the concentration of **2b**.

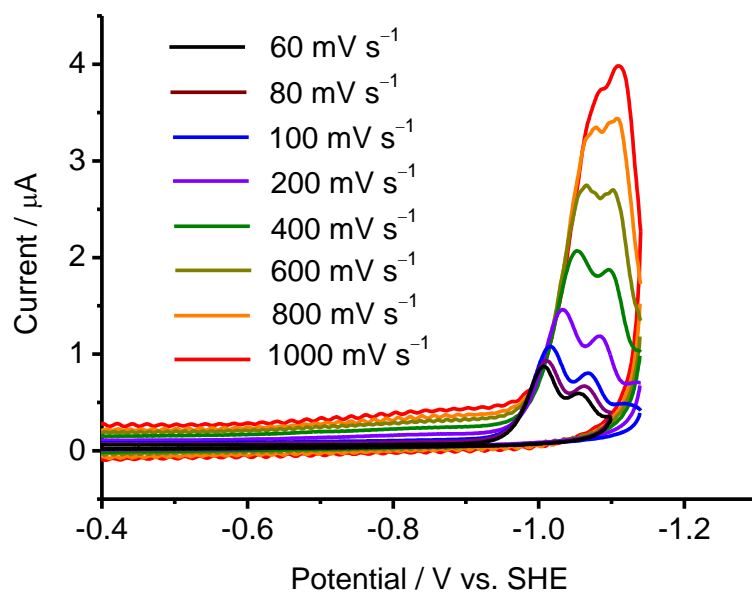


Fig. S16 Cyclic voltammograms of 15 μM **2b** in 1.0 M phosphate buffer at pH 7 with a controlled growth mercury drop electrode at different scan rates.

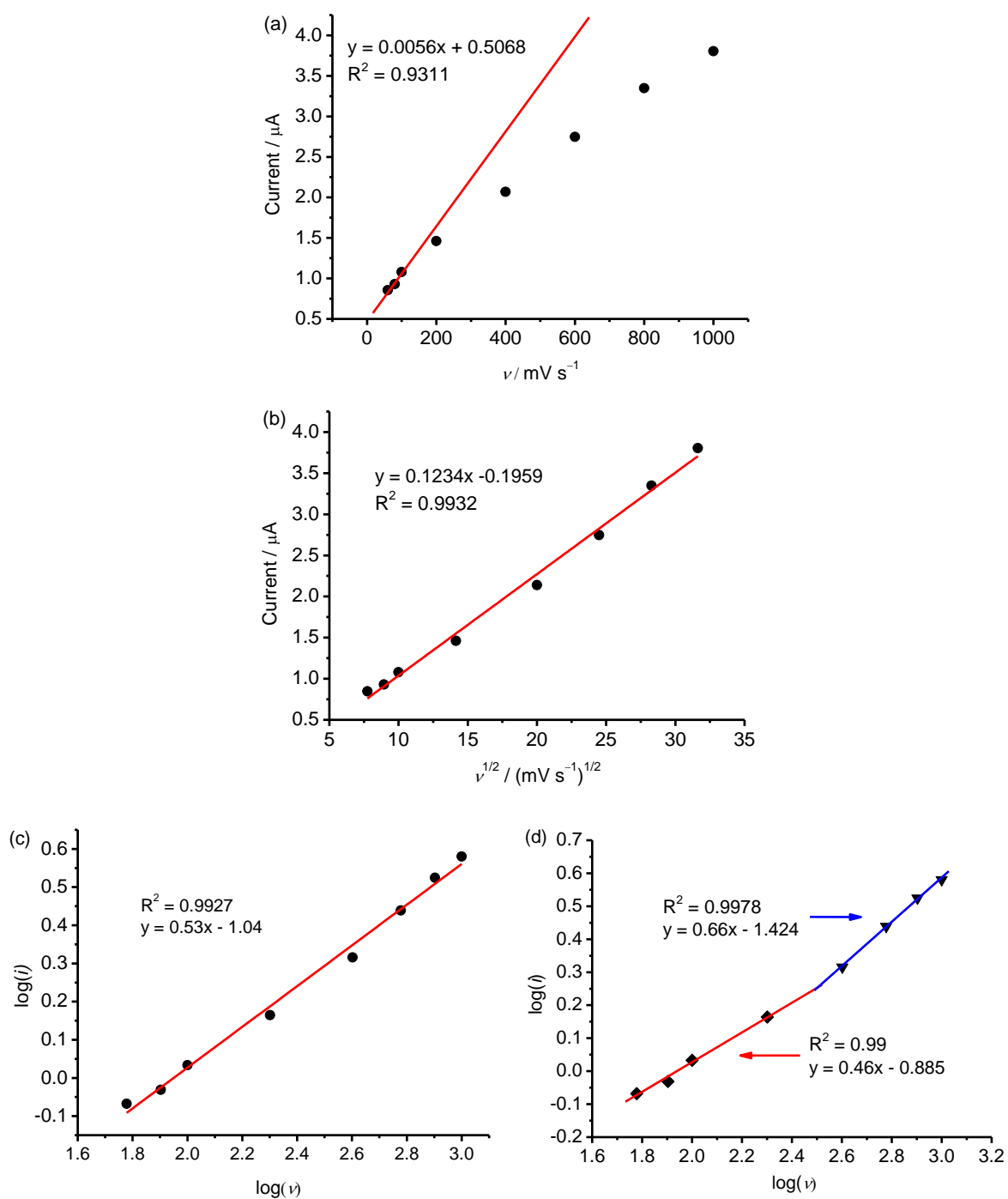


Fig. S17 Plots of the current of first reduction peak at -0.98 V vs. (a) scan rate and (b) the root of scan rate for $15 \mu\text{M}$ **2b** in pH 7 phosphate buffer solutions; Plots of $\log(i)$ vs. $\log(v)$, (c) all data are fit with one line and (d) the two sets of data, with scan rates lower than 200 mV s^{-1} or higher than 500 mV s^{-1} , are fit separately with two lines.

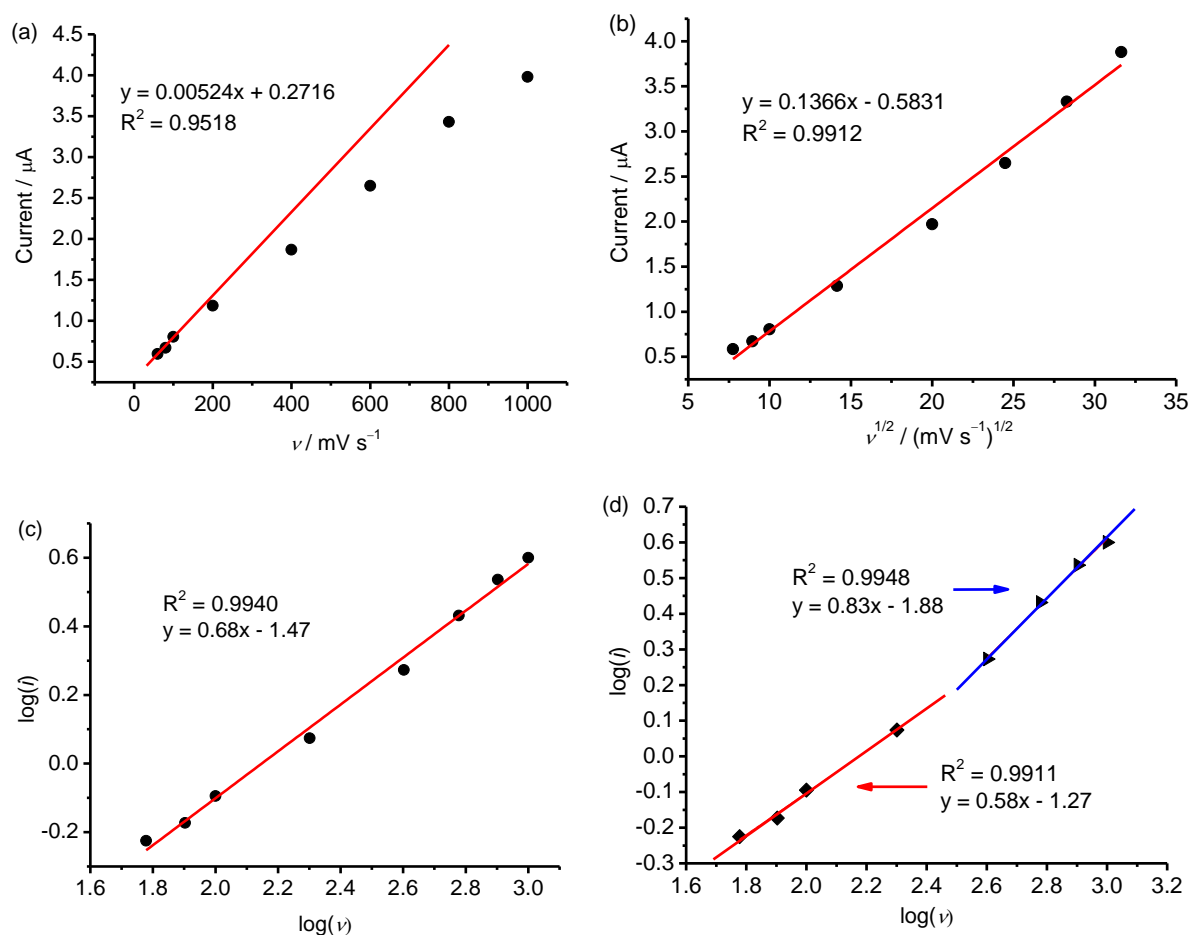


Fig. S18 Plots of the current of second reduction peak at -1.05 V vs. (a) scan rate and (b) the root of scan rate for $15 \mu\text{M}$ **2b** in pH 7 phosphate buffer solutions; Plots of $\log(i)$ vs. $\log(v)$, (c) all data are fit with one line and (d) the two sets of data, with scan rates lower than 200 mV s^{-1} or higher than 500 mV s^{-1} , are fit separately with two lines.

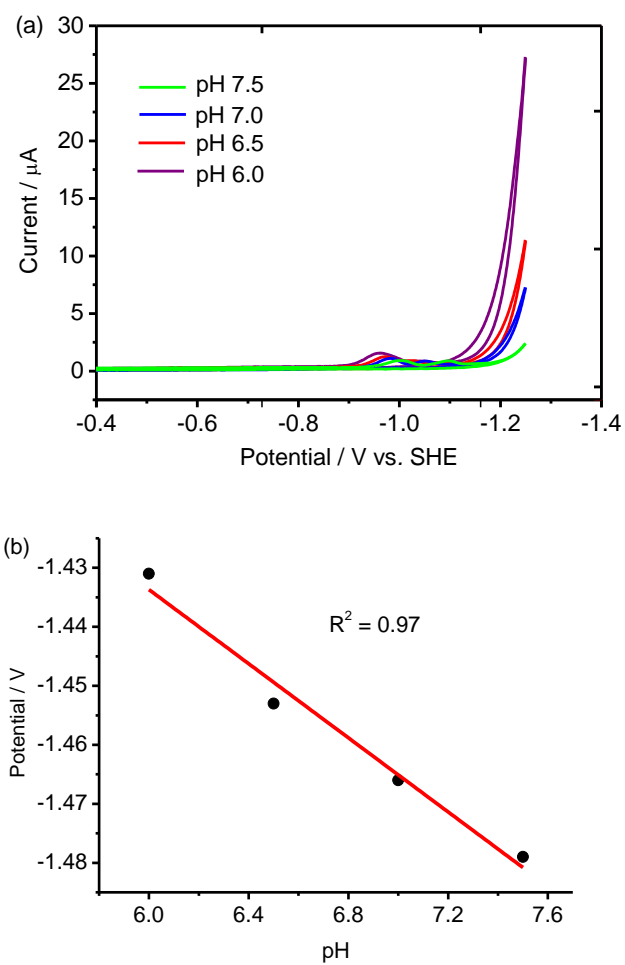


Fig. S19 (a) Cyclic voltammograms of 15 μM **2b** in 1.0 M phosphate buffer at pH 6.0, 6.5, 7.0, 7.5 with a controlled growth mercury drop electrode; (b) Plots of the reduction current versus pH value.

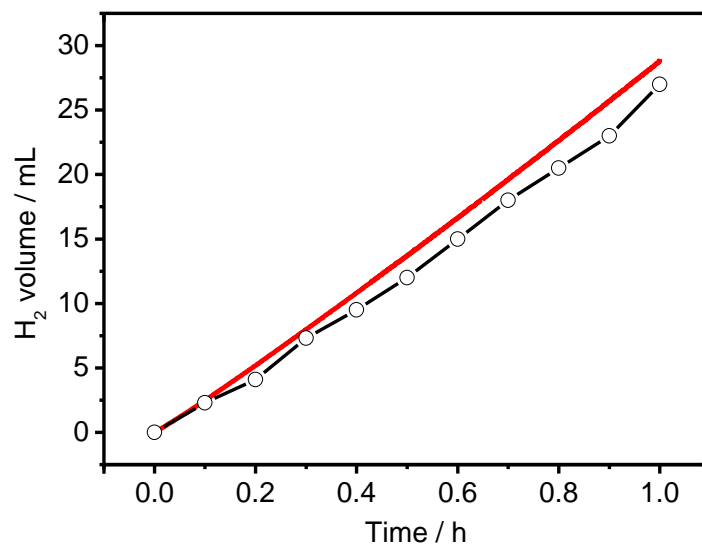


Fig. S20 The amount of hydrogen calculated from passed charge (red solid), assuming a Faradaic efficiency of ~91%, and measured from gas chromatography (white circle) during the electrolysis of 5 μM **2b** in 1.0 M phosphate buffer at pH 7 with an applied potential of -1.25 vs. SHE on a Hg pool electrode.

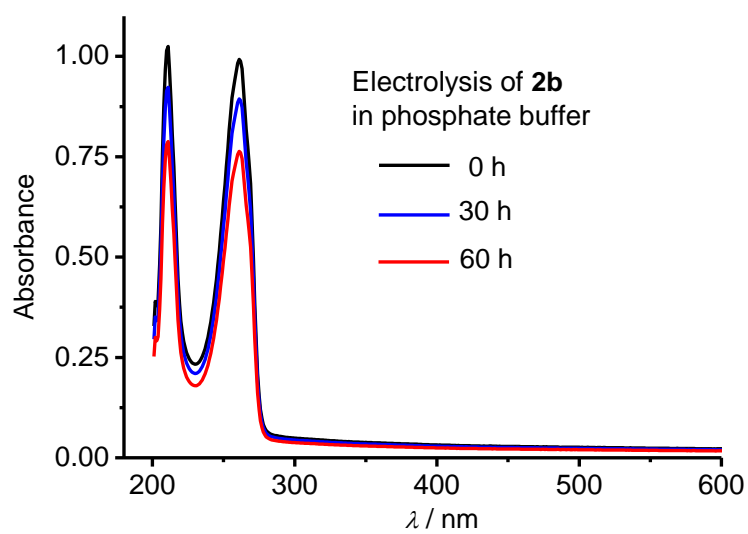


Fig. S21 UV-vis spectra of the aqueous solution of **2b** after electrolysis for 30 and 60 h in a pH 7 phosphate buffer (2.0 M) at an applied potential of -1.25 V on a mercury pool electrode.

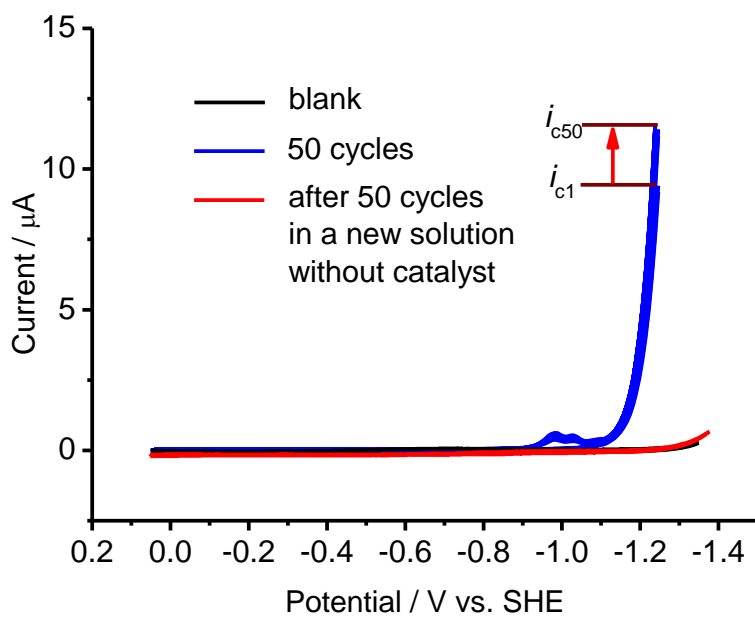


Fig. S22 Cyclic voltammograms of **2b** (15 μM) in 1.0 M phosphate buffer at pH 7 with a controlled growth mercury drop electrode in a scan rate of 100 mV s^{-1} (blue, CV of the 50th cycle of **2b**; red, CV of the working electrode in a fresh phosphate buffer solution in the absence of catalyst after used for 50 cycles; black, CV of 1.0 M phosphate buffer at pH 7).